Ocean Sci. Discuss., 10, 2053–2083, 2013
www.ocean-sci-discuss.net/10/2053/2013/
doi:10.5194/osd-10-2053-2013

Ocean Science
Discussions
Open Access

On the tides and resonances of Hudson Bay and Hudson Strait

D. J. Webb

National Oceanography Centre, Southampton SO14 3ZH, UK

Received: 30 September 2013 – Accepted: 21 October 2013 – Published: 5 November 2013

Correspondence to: D. J. Webb (djw@soton.ac.uk)

Published by Copernicus Publications on behalf of the European Geosciences Union.

Abstract

The resonances of Hudson Bay, Foxe Basin and Hudson Strait are investigated using a linear shallow water numerical model. The region is of particular interest because it is the most important region of the world ocean for dissipating tidal energy.

The model shows that the semi-diurnal tides of the region are dominated by four nearby overlapping resonances. It shows that these not only affect Ungava Bay, a region of extreme tidal range, but they also extend far into Foxe Basin and Hudson Bay and appear to be affected by the geometry of those regions. The results also indicate that it is the four resonances acting together which make the region such an important area for dissipating tidal energy.

1 Introduction

In his study of tidal dissipation on the world ocean, Miller (1966) estimated that Hudson Bay and the Labrador Sea dissipated 140 GW of M2 tidal energy. This made it the fifth most important region of tidal dissipation, the first four being the Bering Sea, the Sea of Okhotsk, the north-west Australian Shelf and the European Shelf.

More recent studies have completely changed this picture. Le Provost and Rougier (1997), using a numerical model, found that the M2 tide dissipated 313 GW in the Hudson Bay region. This made it their most important region for tidal dissipation.

Egbert and Ray (2001) assimilated satellite altimeter into an ocean model and again found the Hudson Bay region to be the most important, the M2 tide dissipating 261 GW. Next in importance was the European Shelf (~208 GW), followed by the north-west Australian Shelf (~158 GW), the Yellow Sea (~149 GW) and the Patagonian Shelf (~112 GW).

The importance of the Hudson Bay complex is also emphasised if one plots the M2 energy flux vectors for the North Atlantic. This has been done in Fig. 1, making use of the satellite derived tidal fields of Egbert and Erofeeva (2002). In the eastern North

OSD
10, 2053–2083, 2013

Atlantic the figure shows a northward flux of tidal energy associated with a propagating Kelvin wave. Part of the energy is lost to the European shelf but a large amount continues north. It then turns westwards and passes south of Greenland before converging on Hudson Strait.

If the fluxes of Fig. 1 are integrated along lines between 44° W 42° N and the coasts of Spain and Greenland, the results show that the M2 tide fluxes 490 GW northwards into the north-east Atlantic and that 220 GW passes south of Greenland towards Hudson Strait. At the entrance to Hudson Strait the flux of energy is 250 GW – the increase being due to local input and a small northward flow of tidal energy on the western side of the Atlantic.

Thus not only is the Hudson Bay complex the major tidal dissipation region of the global ocean, it is also so effective that no energy transporting Kelvin wave continues southwards along the coast of Labrador and Newfoundland. This is in marked contrast to the behaviour on the eastern side of the ocean where a large fraction of the energy flux continues past the resonant European Continental Shelves.

Continental shelf regions with large amounts of tidal dissipation are usually associated with resonances of the shelf. Examples are the Bristol Channel (Fong and Heaps, 1978; Webb, 2013a), the Patagonian Shelf (Huthnance, 1980) and the north-west Australian Shelf. Such regions are usually associated with high tides, so one possible reason why Hudson Bay was overlooked is that it is only recently that Leaf Bay, part of Ungava Bay[1] near the entrance to Hudson Strait, has been reported as having the world's second highest tidal range (O'Reilly et al., 2005).

The high tides of Ungava Bay were studied by Arbic et al. (2007) using a time dependent numerical model. This showed that the tides of the region were affected by a quarter wavelength resonance between the coast and the deep ocean. The resonance mode also showed maxima elsewhere in Foxe Basin and Hudson Bay which,

[1]Leaf Bay is adjacent to Hopes Advanced Bay, indicated by the letter U in Fig. 2. Other locations discussed in the text are also shown in this figure.

OSD
10, 2053–2083, 2013

following the recent study of the English Channel and Irish Sea (Webb, 2013a), might indicate the presence of additional resonances affecting the tides.

The English Channel and Irish Sea study used a time independent model. This has the advantage that it can be run for complex values of angular velocity and so allows a detailed investigation of the resonant structure of a region. In this paper a similar model is used to study the Hudson Bay region. As well as learning more about the resonances, a second aim of the study is to investigate the impact of three unusual properties of the region.

The first of these concerns Hudson Strait. With central depths of over 300 m, the strait is much deeper than is normal for continental shelf regions. The extra depth means that tidal wavelengths are longer than normal and frictional effects are smaller. As a result there is a potential for quarter and three quarter wavelength resonances extending far into Hudson Bay in the south and into Foxe Basin in the north.

A second concerns the complex pattern of bays and channels in Foxe Basin. These all have the potential for supporting resonances and introducing extra complexity into the system.

Finally the open region of Hudson Bay in the south is large enough to support a circulating wave. This may act like a resonator but a damped circulating wave might also have the properties of a damped infinite channel.

Section two of the paper gives the details of the model used for the study. Section three then reports on the results obtained using real values of angular velocity and section four extends this to complex values of angular velocity. Section five is concerned with the main resonances affecting the semi-diurnal tides and section six investigates how these combine to generate the observed response within the tidal band. Finally the discussion section reviews the main results of this study and considers their implications.

OSD
10, 2053–2083, 2013

2 The numerical model

The model used to study the Hudson Bay, Hudson Strait and Foxe Basin region is based on that described by Webb (2013a). It solves the linear form of Laplace's tidal equations at a single angular velocity using finite difference equations based on an Arakawa-C grid distribution of model variables.

The model covers the region bounded by the latitude and longitude lines at 94.25° W, 57.5° W, 51.125° N and 70.375° N, with a resolution of 0.125° in the east-west direction and 0.25° in the north-south direction. The other free parameters are the linear coefficient of bottom friction and the minimum cell depth. These were set to 0.2 cm s^{-1} and 2.5 m, as in Webb (2013a)[2].

Coastlines and cell depths are based on the GEBCO coastline depth data sets (IOC et al., 2003). The GEBCO depth data is at a higher resolution (1/60°) than that used for the model grid, so depths were calculated such that the volume of each model grid cell is the same as the corresponding GEBCO region. Away from coastlines this is equivalent to them having the same average depth.

The open boundary includes part of the Labrador Sea with depths extending down to 3000 m. In this region of the model the northern and southern limits are at 57.125° N and 66.875° N. As a result the open boundary in the east includes almost all of the energy inflow region shown in Fig. 1.

For the open boundary, Webb (2013a) used Dirichlet boundary conditions in which the tidal height on the boundary is fixed. For the present study the model has been modified to allow radiation of energy back into the deep ocean using a method related to that of Webb (2013b). The scheme is based on that proposed by Flather (1976) which is often used for time dependent models. Details are given in Appendix A1.

[2]The model allows the linear coefficient of bottom friction to be a function of position. As discussed by Hunter (1975) this allows the mean effect of a realistic non-linear bottom friction term to be included. Hunter's method requires additional runs of a fully non-linear model and has not be used for the study reported here.

OSD
10, 2053–2083, 2013

3 The M2 tide

The model was validated using a simulation of the M2 tide. For this the model was forced at the open boundary with tidal amplitudes and phases taken from a global assimilation of satellite altimeter data (Egbert and Erofeeva, 2002). The model result is shown in Fig. 2 and the values at representative stations compared with tidal observations in Table 1.

The agreement is good at Hopes Advance Bay, in the west of Ungava Bay near Leaf Basin. The phase in the deep ocean is around 300° so the coast here is approximately 70° out of phase. Given that some of the highest tides in the world are found in Leaf Basin, this phase difference between the coast and the deep ocean is less than the 90° expected from a pure quarter wavelength resonance.

Agreement is also good at Churchill in the far west of Hudson Bay and, after the tidal wave has propagated around the south of Hudson Bay, the reduction in amplitude is represented reasonably well at Great Whale River in the south-east. However the model tide arrives there early. This may indicate that the model depths are too deep or it may be because the model is not correctly representing the nearby amphridrome.

Unfortunately in the north of the model region, analyses are available from only three stations and these are based on only a month's data. Two of these Repulse Bay and Hall Beach are included in the table. The third, Rowley Island, lies close to Hall Beach.

At both Repulse Bay and Hall Beach the model amplitude is not unreasonable but the phase is almost 180° out of agreement. Two series of tests were carried out to see if the difference could be understood.

In the first, the model was run with different values of the friction coefficient. This was found to affect the amplitude at inland stations but have only a small effect on phase. Thus halving the friction coefficient increased the amplitude at Churchill by over 50 % but only changed the phase by 11°. At Repulse Bay the increase was over 150 % and the phase change 12°.

OSD
10, 2053–2083, 2013

The second set of tests arose from the observation that model phases close to the observed phase at Repulse Bay were found in the south-west of Fox Basin. There is also a minimum amplitude in the channel joining the two regions and an area of rapid phase change, implying the presence of an amphidrome or nearby virtual amphridrome.

As the channel may have been too small in the model, tests were carried out where this was made wider and had its shallows removed. The changes affected the amplitude at Repulse Bay but had very little effect on the phases or the position of the amphridrome. A 180° phase change at Repulse Bay only appears possible if the amphridrome is moved to the channel running south towards Hudson Bay.

The phase agreement at Churchill indicates that amplitudes and phases are good in Hudson Bay, so the amphridrome can only be moved if the depths in the south of Fox Basin are increased to raise the speed of the tidal wave through the region. Similarly the phase error at Hall Beach, which is also in a region of low amplitudes, may be explained if the position of the model amphidrome is incorrect due to errors in model depths.

Good depth data from Fox Basin is limited, as it is covered in ice for much of the year, so there is little further that can be done at this stage. However these model phase errors need to be kept in mind in the rest of this analysis.

4 The response at real values of angular velocity

For the remainder of the study, the model was forced at the open boundary with an incoming wave of unit amplitude. Figure 3 shows the amplitude of the resulting model response at representative points within the region plus the amplitude of the outgoing wave at one point on the open boundary.

The chosen locations include Ungava Bay, Repulse Bay and model points R2 and R3. The latter two are on the north side of Hudson Strait and the east side of Foxe Basin where the model semi-diurnal tides are highest. A station in north Fox Basin

OSD
10, 2053–2083, 2013

is also included because the response there appears to be very different to that of east Foxe Basin. In the south, the figure includes Churchill, on the western shore of Hudson Bay, but stations further south are omitted as the responses there are similar to Churchill but with lower amplitudes.

Finally, the figure includes the outgoing wave at point R1 on the open boundary (see Fig. 2). This is chosen because it is in deep water at the foot of the continental slope and is in a position where it should give an indication of the behaviour of Kelvin waves travelling south out of the model region. It also lies near the positions where the resonances, discussed later, show the maximum energy losses through the open boundary.

At zero angular velocity both the ingoing and outgoing waves at the open boundary have unit amplitude, so the amplitude everywhere equals two. As angular velocity increases, the amplitudes initially tend to decrease but they then increase to maxima near the semi-diurnal tidal band. There is then a general decrease to minima around 21 rad day^{-1} after which there are further maxima between 25 and 30 rad day^{-1}.

Within this large scale behaviour there are many individual maxima and changes in curvature, which, on the basis of previous work, are likely to be due to individual resonances or groups of resonances. Sometimes the maxima and changes in curvature occur at the same angular velocity, indicating that such regions are coupled and affected by the same resonance. However at other angular velocities the same regions may have very different response to the forcing.

A noticeable feature of the outgoing wave at R1 is that has a minimum where the resonances are largest near 12 rad day^{-1} and a maximum near 22 rad day^{-1} where the large scale response is least. It then has another minimum near 26 rad day^{-1} where Ungava Bay has a maxima.

An alternative view of the system's response is obtained by plotting the real and imaginary components of the response function, as in Fig. 4. At Ungava Bay the response function contains four main loop structures, two small ones generating the am-

OSD
10, 2053–2083, 2013

plitude minima near 2 and 21 rad day^{-1} and two larger ones, the maxima near 13 and 26 rad day^{-1}.

The outgoing wave at R1 also shows large and small loops at roughly the same angular velocities, but this time the large loops reduce the amplitude of the radiated wave. Near 12 rad day^{-1} the amplitude drops to near 0.1, and as the radiated power depends on the square of the amplitude it implies that the radiated power is close to 1 % of the incident power.

5 The response at complex values of angular velocity

The previous figures illustrate the type of information that can be obtained with models that can investigate real values of angular velocity. However an advantage of the present model is that it can also obtain solutions for complex values of angular velocity and thus explore the full resonant structure of the system.

Figures 5 to 7 show the response function at four stations plotted on the complex plane. In these figures the vertical coordinate indicates the response function amplitude and the colour represents phase, zero phase being the phase of the incoming wave on the open boundary.

Ungava Bay (Fig. 5) is chosen because it appears to support a quarter wavelength resonance. Churchill and location R3 (Fig. 6) are chosen to represent Hudson Bay and Foxe Basin. Location R1 (Fig. 7) lies beyond the outer edge of the continental slope and is chosen to capture any Kelvin wave progressing southward out of the model region.

In the limit of zero angular velocity, both the incoming and outgoing wave on the open boundary have unit amplitude. As a result, as shown in Figs. 5 and 6, the amplitude at the origin is two. Figure 7 shows only the outgoing wave on the boundary, so its amplitude at the origin is one.

As angular velocity increases there is a complex of resonances extending to near 6 rad day^{-1}. As in Webb (2013a) the resonances here are continental shelf and Rossby wave modes. The figures then show a series of gravity wave modes extending to higher

OSD
10, 2053–2083, 2013

angular velocities. The angular velocities of these modes, calculated using the method outlined in Appendix A2, are given in Table 2.

Near the real axis, the colours show that the phase at Ungava Bay increases slowly reaching 90° in the region of the semi-diurnal tides. In contrast there is a more rapid phase change at both Churchill and at location R3, the colours indicating that near the semi-diurnal band these phases are approximately 450°, i.e. one and a quarter wavelengths different from the forcing.

The response function for Ungava Bay shows that the large amplitude region near the semi-diurnal tidal band (12 rad day^{-1}) is associated with four main resonances. These are resonances D to G of Table 2. The figures show that the same resonances are also responsible for large amplitudes in Hudson Bay and Foxe Basin, the strength of individual resonances there often being larger than in Ungava Bay.

In some ways this result is surprising. Ungava Bay is known to have high tides and given the local bathymetry and distance from the shelf edge and the phase of the response function, the high semi-diurnal response might be expected to be due to a single quarter wavelength resonance. Hudson Bay and Foxe Basin are much further from the shelf edge and on the same basis they must involve at least three-quarter wavelength resonances and possibly one and a quarter wavelength resonances.

At higher angular velocities the Ungava Bay response function shows two further strong resonances. The first, resonance Q near 21 rad day^{-1}, has little impact on the response at real values of angular velocity. The second, resonance U near 27 rad day^{-1}, has a much greater impact on the response in Ungava Bay. It is also responsible for an increased amplitude at Churchill but has essentially no impact at position R3. Further investigation of their structure showed that resonance Q is primarily a quarter wavelength resonance of Cumberland Sound and U a similar resonance of Frobisher Bay.

5.1 Radiation at the open boundary

Figure 7 indicates that the first of the large loops in Fig. 4b is associated with resonances D to G and the second large loop with resonance U. The first of the small loops

OSD
10, 2053–2083, 2013

is associated with the shelf and Rossby wave resonances. The cause of the second loop is not so clear but it is likely to be Q together with K and L.

In the previous study of the English Channel and Irish Sea (Webb, 2013a), the high semi-diurnal tides in the Bristol Channel were found to result from two resonances which both had slightly higher angular velocities. It was assumed that these were also responsible for the large amount of tidal energy that was dissipated in the region.

The present result indicates that the strong absorption of tidal energy by the Hudson Bay system is a result of four resonances which straddle the tidal bands. The strong absorption thus may result from straddling the tidal bands or it may result from the fact that four resonances are involved, each of which can provide an independent contribution to resonant absorption of tidal energy.

6 Structure of the main semi-diurnal resonances

The spatial structures of the four largest resonances near the semi-diurnal tidal band were calculated using the method outlined in Appendix A2. The results are shown in Fig. 8. The solutions have been normalised so that the maximum amplitude is one and the phase is zero in the west of Ungava Bay. For two of the modes, the maxima are on the eastern side of Foxe Basin. The other two have maxima on the western side of James Bay.

Plots of energy flux vectors show that in each case the energy flux is away from the deep regions of Hudson Strait, both eastwards towards the open boundary and westwards towards the high amplitude regions in Foxe Basin or Hudson Bay.

None of the modes can be characterised by a single unique feature, such as a standing wave in a limited region of shelf. Instead they appear to involve the coupling of a series of such simple or underlying modes.

The first of these is the quarter wavelength resonance involving Ungava Bay. The justification for this is the fact that all four modes show an approximate 90° phase lag

OSD
10, 2053–2083, 2013

between the west side of Ungava Bay and the shelf edge or open boundary – although depending on the precise point chosen the value can vary between 75 and 130°.

A second is a three-quarter wavelength mode between the shelf edge or open boundary and the east side of Foxe Basin. As seen best in resonance E, this has a quarter wavelength maximum in Hudson Strait and a half wavelength node to the north of Southampton Island.

A third is a half wavelength resonance trapped between the north-west and south-east coasts of Foxe Basin. This is best seen in resonance D, but as the model had poor agreement with the measured tide in the NW of Foxe Basin, this possibility should be treated with caution.

Finally, Hudson Bay itself appears to support a single wavelength wave that circles the bay in an anti-clockwise direction. This is best seen in resonance F.

The results imply that although resonances involving the shelf edge are important, the grouping of resonances around the semi-diurnal tides is partly due to standing waves within the interior of the Hudson Bay system.

7 Resonant contributions near two cycles per day

As discussed in Webb (2012), the response function near a tidal band can be split into the contribution of nearby resonances and a smooth background due to distant resonances. Thus,

$$R(x,\omega) = \sum_j R_j(x)/(\omega - \omega_j) + S(x,\omega) + B(x,\omega) \ , \qquad (1)$$

where $R(x,\omega)$ is the response function at position x and angular velocity ω. The sum j is over key nearby resonances and $R_j(x)$ is the residue at ω_j, the resonance angular velocity. Methods for calculating the residue are described in Appendix A3. The symmetry term $S(x,\omega)$ is not essential but it is easy to calculate and represents the contribution

OSD
10, 2053–2083, 2013

from the conjugate set of resonances, i.e. the contribution from resonances at $-\omega_j^*$. $B(x,\omega)$ is the smooth background due to distant poles.

In Fig. 9, this equation has been used to determine how the four resonances of Fig. 8 contribute to the high semi-diurnal tides of Ungava Bay and the low outgoing wave at position R1 on the open boundary.

It shows that in Ungava Bay the high tides are primarily due to resonances F and G. They both have large amplitudes and, as their phases are similar, they reinforce each other. Resonance E makes some contribution, but D is insignificant, its amplitude being smaller than the background.

Resonances F and G are also the dominant ones at position R1. At 12 rad day^{-1} they both have the effect of reducing the amplitude of the outgoing wave by about a third. At the same point resonances D and E are contributing to a reduction of the outgoing wave, but by 13 rad day^{-1} this is no longer the case.

The net effect of the resonances at 12 rad day^{-1} is to reduce the response function amplitude from 0.91 to 0.15. Assuming the power is proportional to the amplitude squared this means that the four resonances are absorbing over 97 % of the incident tidal energy. Resonances F and G together reduce the energy by approximately 90 % and although the contributions of resonances D and E are much smaller they are responsible for absorbing over 70 % of the remaining energy.

8 Conclusions

The study has shown that the semi-diurnal tides of the Hudson Bay region are dominated by four resonances. These straddle the semi-diurnal tidal band and contribute both to high tidal amplitudes within the region and to very low amplitudes in the tidal wave radiated away from the region.

The previous study, made using a time dependent model (Arbic et al., 2007), was only able to identify one resonance affecting the semi-diurnal tides. The new result therefore emphasizes the usefulness of the present approach.

OSD
10, 2053–2083, 2013

The study does not explain why the Hudson Bay system is such a good absorber of tidal energy and more effective than the English Channel and Irish Sea but it does give hints that need to be followed up.

The first is the primary result that the Hudson Bay system has four significant resonances close to and straddling the semi-diurnal tidal band. In the case of the Bristol Channel and Gulf of St Malo there are only two resonances and they lie to one side of the tidal band.

The study also used one of the points on the open boundary as an analogue of the reflected wave for the case of a uniform amplitude incident wave at all points on the open boundary. Although the uniform amplitude incident wave is a special case, it is a plausible first approximation to the way the M2 tide forces the region.

The results show that each of the four main resonances acted to reduce the amplitude of the reflected wave in the semi-diurnal tidal band. At two cycles per day, two of the resonances together absorbed ~90 % of the incident energy and the other two, although weaker, absorbed ~70 % of the remainder. The small reflection coefficients imply that all four resonances have impedances which are well matched to that of the deep ocean.

The study shows that the closeness of the resonances is partly due to the complex topography of the region. As well as the "classical" 1/4 wavelength wave between Ungava Bay and the shelf edge, the deep Hudson Strait also allows the development of 3/4 wavelength, and possibly 5/4 wavelength, resonances between the shelf edge and features far to the west. There, both Foxe Basin and Hudson Bay are of the right size to support standing waves of near tidal period.

The depth of Hudson Strait also means that energy dissipation is reduced compared with a normal shelf. The mean depth (~300 m) is approximately four times that of a normal shelf (~80 m), so the frictional effect per wavelength in the strait should be halved. This probably helps in matching the Foxe Basin and Hudson Bay components of the resonances to the deep ocean.

OSD
10, 2053–2083, 2013

The effectiveness of a continental shelf region in absorbing tidal energy is also likely to depend on both the length of continental shelf involved and the angle at which the tidal wave approaches the shelf. These features have not been studied here but as it passes the English Channel and Irish Sea, the semi-diurnal tidal wave in the deep ocean runs roughly parallel to the shelf edge. In contrast, as it approaches Hudson Strait the wave approaches roughly at right angles to the shelf edge.

To conclude, the present study has given new insights into the properties of the Hudson Bay region and the complex interactions that are involved. The study has shown that there is still much to be learnt about the physics of the region but the results presented here should provide a useful basis for further work.

Appendix A

A1 Mathematical and numerical details

The model used for the present study is based on Laplace's tidal equations, which are converted into a set of finite difference equations on an Arakawa-C grid, as described in Webb (2013a). The model assumes a time dependence of the form $\exp(-i\omega t)$, where t is time and ω the angular velocity of the ocean wave. If the model variables are represented by a vector $\boldsymbol{y}$, then the finite difference equations can be written in the form,

$$(\mathbf{L} - i\omega\mathbf{1})\boldsymbol{y} = \boldsymbol{z}. \quad \text{(A1)}$$

where $\mathbf{1}$ is the unit matrix. The term $(-i\omega\mathbf{1})$ results from the time dependent terms in Laplace's tidal equations and the matrix $\mathbf{L}$ contains the contributions from all the other terms in the set of finite difference equations. The vector $\boldsymbol{z}$ represents the forcing. If the variables are numbered in a systematic manner, $\mathbf{L}$ becomes a band matrix and the equations can be solved using efficient band matrix algorithms.

OSD
10, 2053–2083, 2013

Equation (A1) represents a linear physical system. Such systems have a number of important properties, one of which is that there exist resonances. The eigenfunction equation corresponding to Eq. (A1) is,

$$(\mathbf{L} - i\omega_i \mathbf{1})\boldsymbol{e}_i = 0. \tag{A2}$$

where ω_i is the ith eigenvalue and $\boldsymbol{e}_i$ is the corresponding eigenvalue.

A2 The open boundary condition

In previous versions of the model, sea surface height (ssh) points on the open boundary were treated explicitly as part of the model vector $\boldsymbol{y}$. However an investigation of the properties of the adjoint system[3] showed that it was better to treat the open boundary condition implicitly, that is as an additional term acting on the normal velocities at points adjacent to the open boundary.

The previous version also used Dirichlet boundary conditions on the open boundary in which ssh on the open boundary is fixed. To allow radiation of energy through the open boundary, a scheme has been developed based on the one proposed by Flather (1976) which is often used for time dependent models.

Let ζ represent sea surface height and u the velocity normal to an open boundary placed at the origin of co-ordinate x. In a plane wave propagating in the positive direction in a region of constant depth h, the sea surface height and velocity are related by

$$u = (c_0/h)\zeta \tag{A3}$$

where the wave speed c_0 equals $(gh)^{1/2}$.

The new boundary condition assumes that the solution in the neighbourhood of a boundary point can be expressed as the sum of two such waves each propagating in

[3]To be published in a technical report.

OSD
10, 2053–2083, 2013

opposite directions normal to the boundary,

$$\zeta = \mathrm{A}\exp(ikx - i\omega t) + \mathrm{B}\exp(-ikx - i\omega t), \tag{A4}$$
$$u = \mathrm{A}(c_0/h)\exp(ikx - i\omega t) - \mathrm{B}(c_0/h)\exp(-ikx - i\omega t),$$

If A represents the unknown outgoing wave and B the known incoming wave, then eliminating A, the open boundary condition becomes,

$$\zeta - (c_0/h)u = 2\mathrm{B}. \tag{A5}$$

As the open boundary value of ζ is not part of the model vector, this equation is used to replace the term involving the open boundary ζ in the equation for the normal velocity point closest to the boundary.

Webb (2013b) proposed a similar scheme but one which allowed for the differing position of the ssh and velocity points. Unfortunately the resulting open boundary condition is a function of ω and as a result the matrix **L** also becomes a function of ω. Tests were carried out with both boundary conditions, to see the effect of the change on the calculated eigenvalues and eigenfunctions. The effect was small, the differences in the calculated resonance eigenvalues being less than 0.01 rad day^{-1}.

A3 Calculation of Eigenvalues and Eigenvectors

Initial estimates of the eigenvalues ω_j were obtained from the datasets used to generate Figs. 5 and 6 by fitting the four points around each maximum of the response function to the expansion,

$$R(\omega) = \mathrm{A}/(\omega - \omega_j) + \mathrm{B} + \mathrm{C}\omega, \tag{A6}$$

Accurate values of the eigenvector and eigenvalue were then obtained by inverse iteration, i.e. by solving the set of equations,

$$(\mathbf{L} - i\omega'_j\mathbf{1})\boldsymbol{e}_j^{[n]} = \boldsymbol{e}_j^{[n-1]}/N_j^{[n-1]} \tag{A7}$$

OSD
10, 2053–2083, 2013

where ω'_j is the initial estimate of ω_j, $\boldsymbol{e}_j^{[n]}$ is the solution of the nth iteration and $N_j^{[N]}$ is a normalising constant equal to the maximum element of vector $\boldsymbol{e}_j^{[n]}$.

The sequence converged to the order of the machine rounding error after less than 10 iterations. Then from Eqs. (A2) and (A7), if $\boldsymbol{e}_j$ is the converged eigenvector and N_j the converged normalisation constant,

$$(\mathbf{L} - i\omega_j \mathbf{1})\boldsymbol{e}_j = 0. \tag{A8}$$
$$(\mathbf{L} - i\omega'_j \mathbf{1})\boldsymbol{e}_j = \boldsymbol{e}_j / N_j.$$

Subtracting the equations, the true eigenvalue ω is given by,

$$\omega_j = \omega'_j - i/N_j. \tag{A9}$$

The results were checked by obtaining the corresponding eigenvectors $\boldsymbol{a}_j$ of the Hermitian adjoint matrix equation with eigenvalue $-\omega_j$. These were then normalised so that the dot product $(\boldsymbol{a}_j^* \boldsymbol{e}_j)$ equalled one. Under these conditions the dot product $(\boldsymbol{a}_j^* \boldsymbol{e}_k)$ should be zero when $j \neq k$. This was found to be correct to within the machine rounding error.

A4 The Residue

In Sect. 7 of the paper, Eq. (1) requires the sea surface height residue $R_j(x)$ of eigenvector j at position x. If $e_{j,k}$ is the eigenvector sea surface height component at this position then the residue is given by the equation,

$$R_j(x) = e_{j,k}(\boldsymbol{a}_j^* z). \tag{A10}$$

where z is the forcing vector, representing the incoming wave at the open boundary and $\boldsymbol{a}_j$ is defined above.

OSD
10, 2053–2083, 2013

The residue can also be obtained from from the inverse iteration sequence (Eq. A7). If the iterations are initialised with $\boldsymbol{e}_j^{[0]}$, equal to z and $N_j^{[0]}$ equal to 1, then after n iterations

$$\boldsymbol{e}_j^{[n]} = \boldsymbol{e}_j^{[n-1]}(\boldsymbol{a}_j^* z)\prod_{k=1}^{n}\left(N_j^{[k]}/N_j^{[n]}\right) + \epsilon, \tag{A11}$$

where ϵ is the contribution from distant resonances. Once the solution has converged, then to within the machine rounding error, ϵ is zero and $\boldsymbol{e}_j^{[n]}$ equals $\boldsymbol{e}_j^{[n-1]}$, so,

$$(\boldsymbol{a}_j^* z) = \prod_{k=1}^{n}\left(N_j^{[n]}/N_j^{[k]}\right), \tag{A12}$$

$$R_j(x) = e_{j,k}\prod_{k=1}^{n}\left(N_j^{[n]}/N_j^{[k]}\right). \tag{A13}$$

References

Arbic, B. K., St-Laurent, P., Sutherland, G., and Garrett, C.: On the resonance and influence of the tides in Ungava Bay and Hudson Strait, Geophys. Res. Lett, 34, L17606, doi:10.1029/2007/GL030845, 2007. 2055, 2065

Egbert, G. D. and Erofeeva, S. Y.: Efficient inverse modeling of barotropic ocean tides, J. Atmos. Ocean. Tech., 183–204, 2002. 2054, 2058, 2075

Egbert, G. and Ray, R.: Estimates of M_2 tidal energy dissipation from TOPEX/Poseidon altimeter data, J. Geophys. Res., 106, 22475–22502, 2001. 2054

Flather, R. A.: A Tidal Model of the north-west European Continental Shelf, Mémoires Société Royale des Sciences de Liége, 10, 141–164, 1976. 2057, 2068

Fong, S. and Heaps, N.: Note on the quarter-wave tidal resonance in the Bristol Channnel, Report No. 63, Institute of Oceanographic Sciences, 15 pp., 1978. 2055

Hunter, J. R.: A note on quadratic friction in the presence of tides, Estuar. Coast. Mar. Sci., 3, 473–475, 1975. 2057

OSD
10, 2053–2083, 2013

Huthnance, J. M.: On shelf-sea resonance with application to Brazilian M3 tides, Deep-Sea Res., 27A, 347–366, 1980. 2055

IHB: Tides, List of Harmonic Constants, Special Publication No. 26, International Hydrographic Bureau, Monaco, 1954. 2073

IOC, IHO, and BODC: Centenary Edition of the GEBCO Digital Atlas, published on CD-ROM on behalf of the Intergovernmental Oceanographic Commission and the International Hydrographic Organization as part of the General Bathymetric Chart of the Oceans, British Oceanographic Data Centre, Liverpool, UK, 2003. 2057

Le Provost, C. and Rougier, F.: Energetics of the barotropic ocean tides: an estimate of bottom friction dissipation from a hydrodynamic model, Prog. Oceanogr., 40, 37–52, 1997. 2054

Miller, G. R.: The flux of tidal energy out of the deep ocean, J. Geophys. Res., 71, 2485–2489, 1966. 2054

O'Reilly, C. T., Solvason, R., and Solomon, C.: Where are the world's largest tides, in: BIO Annual Report: 2004 in Review, edited by: J. Ryan, Biotechnol. Ind. Org., Washington, DC, 44–46, 2005. 2055

Webb, D. J.: On the shelf resonances of the Gulf of Carpentaria and the Arafura Sea, Ocean Sci., 8, 733–750, doi:10.5194/os-8-733-2012, 2012. 2064

Webb, D. J.: On the shelf resonances of the English Channel and Irish Sea, Ocean Sci., 9, 731–744, doi:10.5194/os-9-731-2013, 2013. 2055, 2056, 2057, 2061, 2063, 2067

Webb, D. J.: On the Impact of a Radiational Open Boundary Condition on Continental Shelf Resonances, National Oceanography Centre, Internal Document 06, National Oceanography Centre, Southampton, available at: http://eprints.soton.ac.uk/349401, 2013b. 2057, 2069

OSD
10, 2053–2083, 2013

Table 1. Model M2 tidal amplitude (m) and phases (degrees relative to the equilibrium tide at Greenwich) compared with tide gauge analyses (IHB, 1954).

		Model		Tide Gauge	
		Amp. (m)	Phase °	Amp. (m)	Phase °
Hopes Advance Bay	69.6° W 59.4° N	3.16	13	3.88	10
Churchill	94.2° W 58.8° N	1.46	13	1.52	24
Great Whale River	77.8° W 55.3° N	0.54	345	0.63	17
Repulse Bay	86.5° W 66.4° N	1.63	18	1.88	192
Hall Beach	81.2° W 68.8° N	0.36	186	0.22	25

OSD
10, 2053–2083, 2013

Table 2. Real and imaginary components of angular velocity (in radians per day) for the gravity wave resonances.

	Angular velocity			Angular velocity	
	Real	Imag.		Real	Imag.
A	4.1435	−1.1716	N	19.9437	−2.5796
B	5.1052	−1.6125	O	20.2071	−1.5208
C	7.5167	−1.2326	P	20.9670	−1.8545
D	9,4433	−1.5199	Q	21.4514	−2.1738
E	10.8327	−1.7144	R	23.2567	−1.6131
F	12.1613	−1.5320	S	24.4043	−1.3558
G	13.9215	−1.6782	T	26.1338	−1.6607
H	15.6169	−3.9629	U	26.5379	−1.2928
I	16.0036	−1.5008	V	27.7020	−2.0412
J	16.5089	−4.4841	W	28.7601	−1.1003
K	17.1372	−1.4164	X	28.9116	−1.7231
L	18.2980	−1.2522	Y	29.0517	−4.0404
M	19.7361	−1.5471			

OSD
10, 2053–2083, 2013

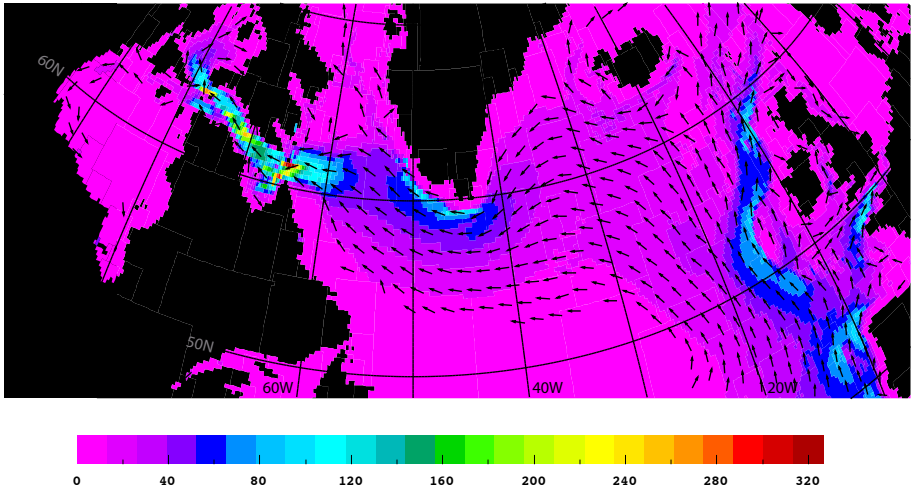

Fig. 1. Energy flux vectors for the M2 tide in the North Atlantic, based on from data from OTIS2 (Egbert and Erofeeva, 2002). Energy flux in units of MW m^{-1}.

OSD
10, 2053–2083, 2013

Tidal Resonances of Hudson Strait

D. J. Webb

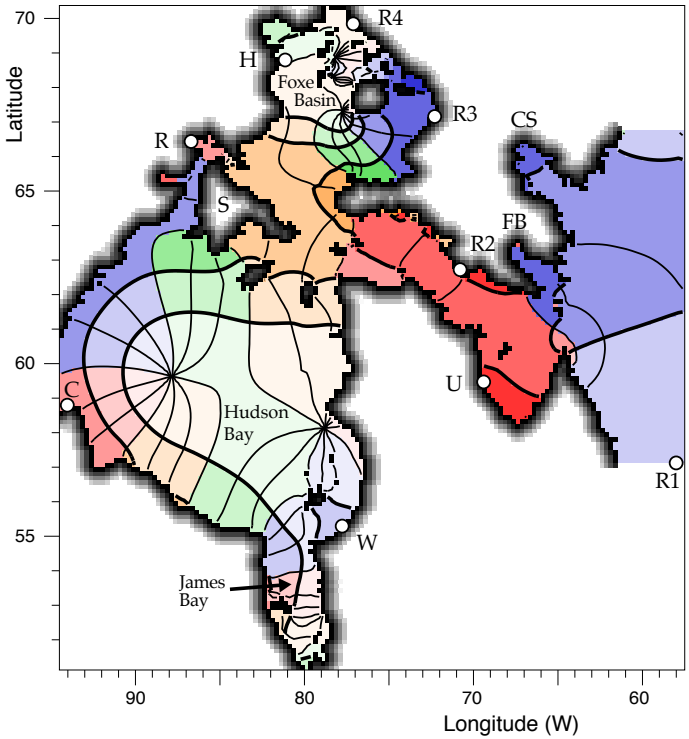

Fig. 2. Model solution for the M2 tide. Thick lines are contours of amplitude at 0.5 m, 1 m, 2 m and 3 m. Thin lines are contours of phase, at intervals of 30°, relative to the equilibrium tide at Greenwich. Colours denote phase quadrant (red, 0°–90°; orange, 90°–180°; green, 180°–290°; blue, 270°–360°) with the more intense colours denoting higher amplitudes. The tide gauge stations are C, Churchill; H, Hall Beach; R, Repulse Bay; W, Great Whale River; U, Hopes Advance Bay (Ungava Bay). Locations R1 to R4, S (Southampton Island), FB (Frobisher Bay) and CS (Cumberland Sound) are referred to elsewhere in the paper.

OSD
10, 2053–2083, 2013

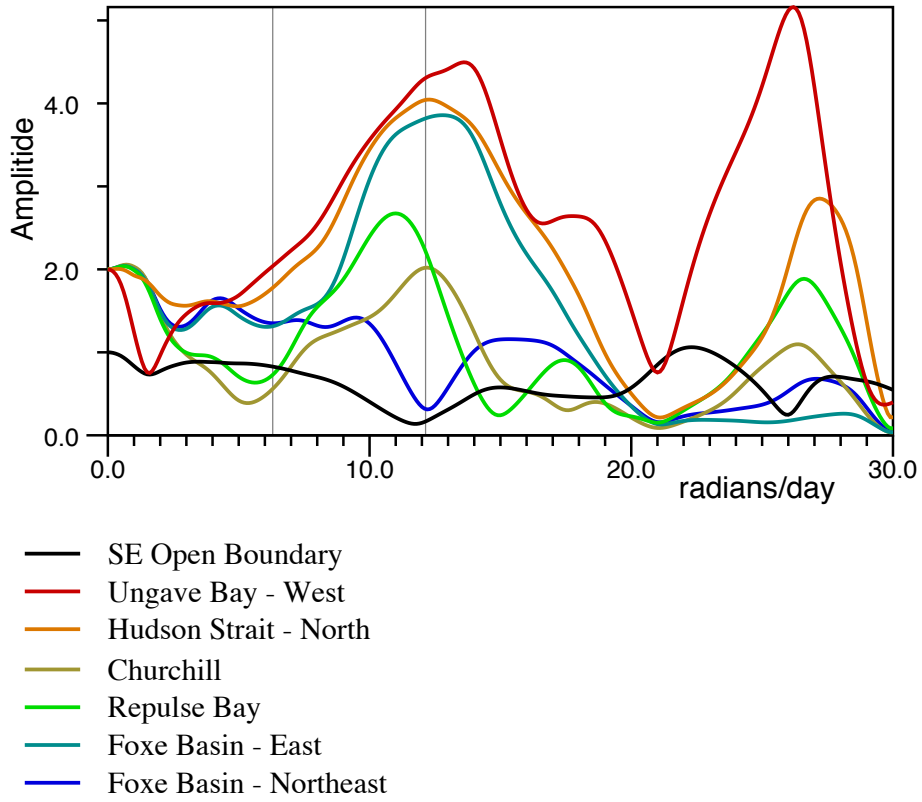

Fig. 3. In colour: amplitude of the response function plotted as a function of angular velocity for real values of angular velocity. Colours: red, Ungava Bay (Hopes Advance Bay); orange, location R2 (see Fig. 1), north side of Hudson Strait; brown: Churchill; green, Repulse Bay; light blue, R3, East Foxe Basin: dark blue, R4, North Foxe Basin. In black: amplitude of outgoing (radiated) wave at boundary point R1.

OSD
10, 2053–2083, 2013

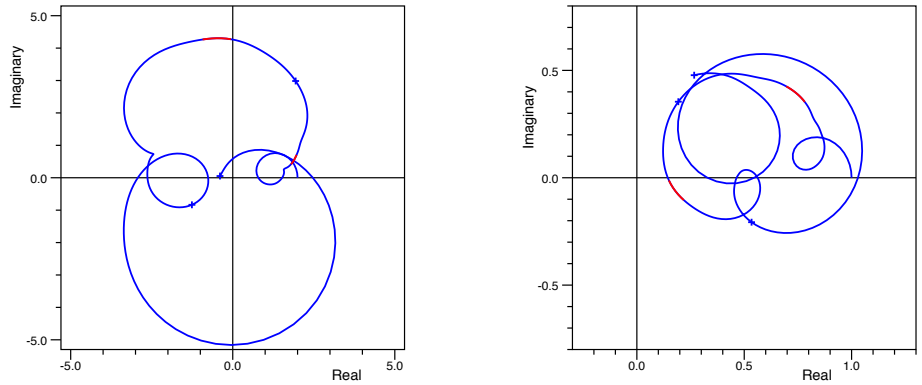

(a) Ungava Bay

(b) Outgoing wave at R1

Fig. 4. Real and imaginary components of **(a)** the response function on the west side of Ungava Bay and **(b)** the outgoing wave at point R1 on the open boundary, plotted for real values of angular velocity between zero and 30 rad day^{-1}. Crosses at intervals of 10 rad day^{-1}. The red sections correspond to the diurnal and semi-diurnal tides. At zero rad day^{-1} the response function at Ungava Bay has the value ($2 + i0$) and the outgoing wave has the value ($1 + i0$).

OSD
10, 2053–2083, 2013

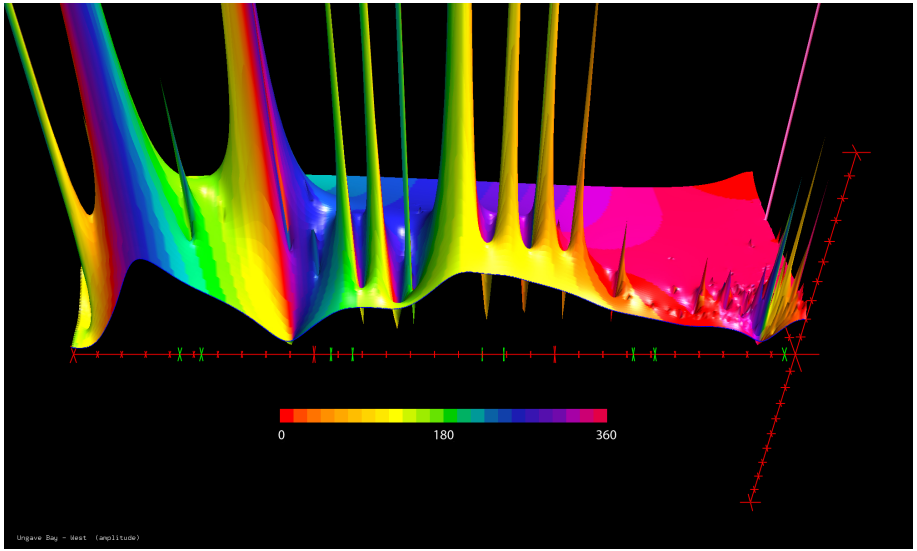

Fig. 5. Response function amplitude on the west side of Ungava Bay plotted as a function of complex angular velocity. The colours denote complex phase, in degrees, as denoted on the scale below the main figure. Values at real values of angular velocity are plotted in blue. The origin (0,0) is on the right with the positive real axis (in red) running from right to left and the negative imaginary axis running into the figure. Both are marked by red crosses every 1 rad day^{-1}. The vertical axis is marked similarly at unit intervals. On the real axis green crosses indicate the limits of the tidal bands near 1 (diurnal), 2 (semi-diurnal), 3 and 4 cycles per day.

OSD
10, 2053–2083, 2013

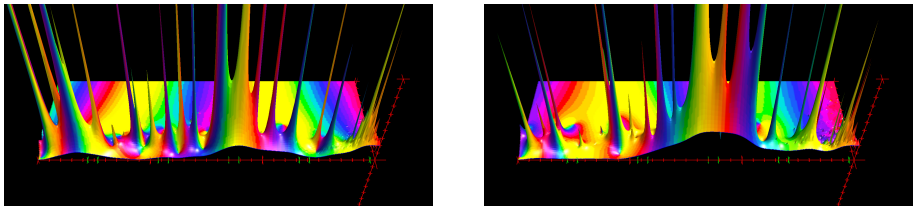

(a) Churchill

(b) R3, east side of Foxe Basin

Fig. 6. The response function amplitude plotted as a function of complex angular velocity **(a)** at Churchill and **(b)** location R3 on the eastern side of Foxe Basin. Colours and axes as in Fig. 5.

OSD
10, 2053–2083, 2013

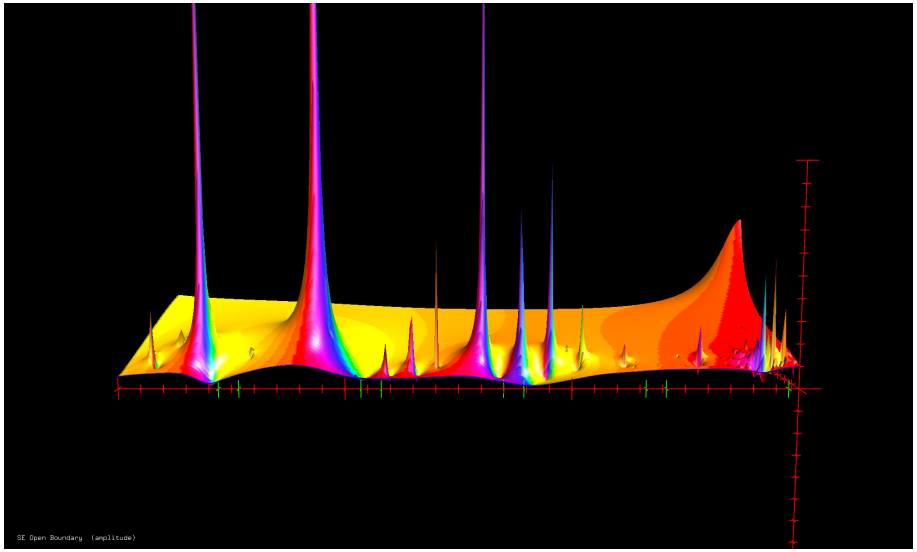

Fig. 7. Response function amplitude of the outgoing wave at point R1 on the open boundary. Colours and scales as in Fig. 5.

OSD
10, 2053–2083, 2013

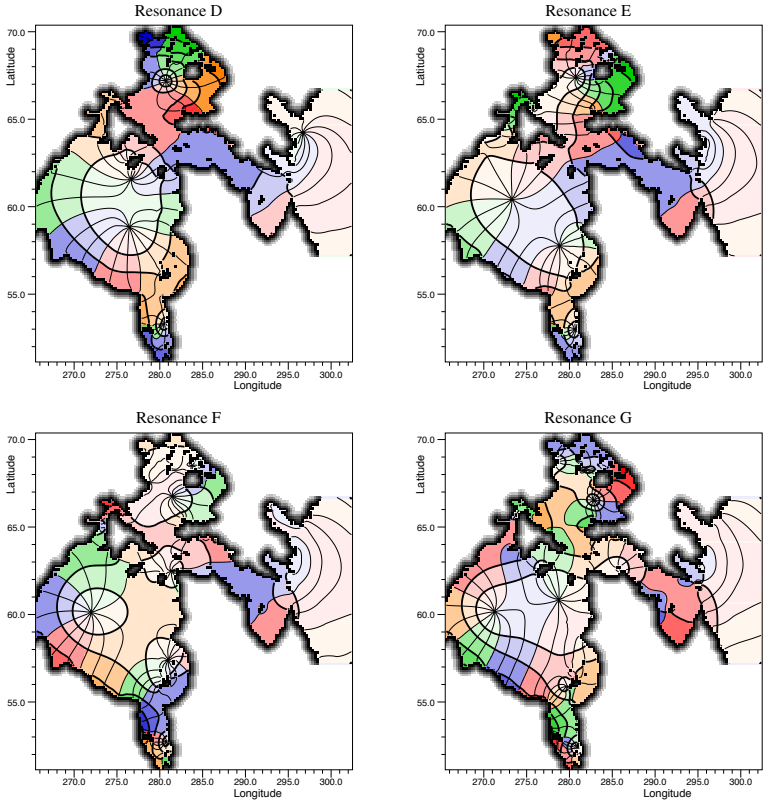

Fig. 8. The amplitude and phase of resonances D to G of Table 2. Amplitudes normalised to one and phases are relative to the west side of Ungava Bay. Thick lines are contours of amplitude at 0.1, 0.2, 0.4, 0.6 and 0.8. Thin lines are contours of phase at intervals of 30°. Colours as in Fig. 1, with zero phase between the red and blue areas.

OSD
10, 2053–2083, 2013

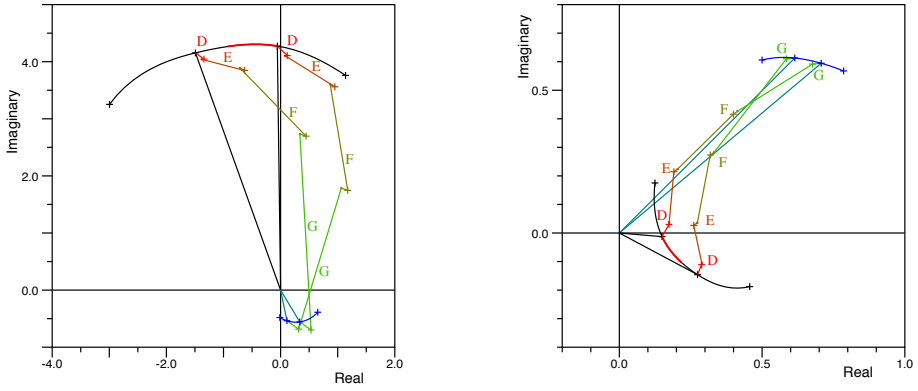

(a) Ungava Bay

(b) Outgoing wave at R1

Fig. 9. In black: real and imaginary components of the response function **(a)** on the west side of Ungava Bay and **(b)** the outgoing wave at point R1 on the open boundary, plotted for real values of angular velocity between 11 and 14 rad day^{-1}. Coloured vectors indicate the contributions of the resonances D to G of Table 2 and their conjugates. The blue line is the residual background. The red section of the main curve corresponds to the semi-diurnal tides.

OSD
10, 2053–2083, 2013

Tidal Resonances of Hudson Strait

D. J. Webb